

**CRACKLING NOISE AND AVALANCHES: SCALING,
CRITICAL PHENOMENA, AND THE
RENORMALIZATION GROUP**

James P. Sethna

*Laboratory of Atomic and Solid State Physics, Cornell University,
Ithaca, NY, USA*

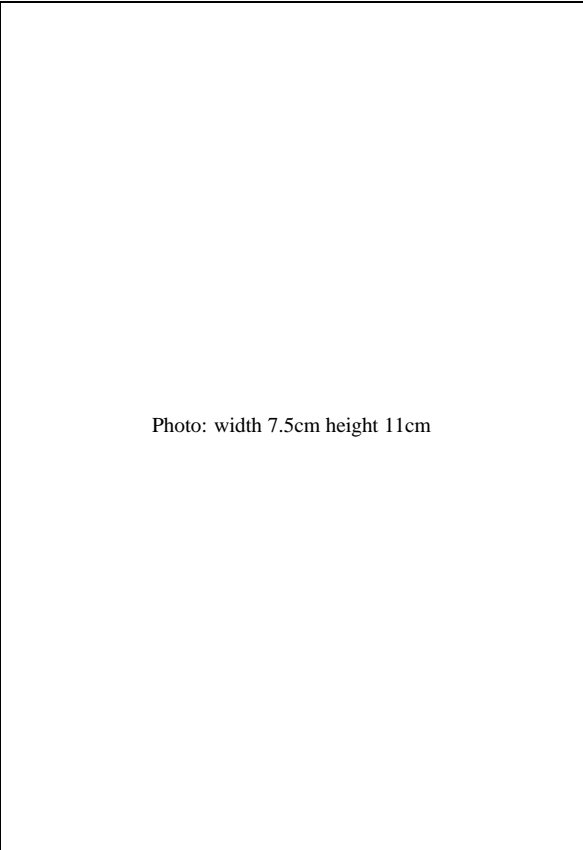


Photo: width 7.5cm height 11cm

Contents

1. Preamble	5
2. What is crackling noise?	5
3. Hysteresis and Barkhausen noise in magnets	7
3.1. Dynamical Random-field Ising model	8
3.2. Real Barkhausen noise	12
4. Why Crackling Noise?	14
4.1. Universality	14
4.2. Renormalization group	18
5. Self-similarity and its consequences	21
5.1. Power laws	23
5.2. Scaling functions	26
5.2.1. Average pulse shape	26
5.2.2. Avalanche size distribution	28
References	31

1. Preamble

In the past two decades or so, we have learned how to understand crackling noise in a wide variety of systems. We review here the basic ideas and methods we use to understand crackling noise—critical phenomena, universality, the renormalization group, power laws, and universal scaling functions. These methods and tools were originally developed to understand continuous phase transitions in thermal and disordered systems, and we also introduce these more traditional applications as illustrations of the basic ideas and phenomena.

We focus largely on crackling noise in magnetic hysteresis, called *Barkhausen noise*. These lecture notes are distilled from a review article written with Karin Dahmen and Christopher Myers [1], from a book chapter written with Karin Dahmen and Olga Perković [2], and from a chapter in my textbook [3].

2. What is crackling noise?

Many systems, when stressed or deformed slowly, respond with discrete events spanning a broad range of sizes. We call this *crackling noise*. The Earth crackles, as the tectonic plates rub past one another. The plates move in discrete earthquakes (Fig. 1a), with many small earthquakes and only a few large ones. If the earthquake series is played as an audio clip, sped up by a factor of ten million, it sounds like crackling [4]. A piece of paper [6] or a candy wrapper [10] will crackle as it is crumpled (try it!), emitting sharp sound pulses as new creases form or the crease pattern reconfigures (Fig. 2(a)). Paper also tears in a series of avalanches [7]; fracture in many other systems exhibit avalanche distributions and jerky motion [11, 12]. Foams (a head of beer) move in jerky avalanches as they are sheared [13], and as the bubbles pop [14]. Avalanches arise when fluids invade porous media in avalanches [15, 16] (such as water soaking into a sponge). I used to say that metals were an example of something that did not crackle when bent (permanently plastically deformed), but there is now excellent data that ice crackles when it is deformed [8], and recent data on micron-scale metal deformation also shows crackling noise [17, 18]. We will focus here on *Barkhausen noise*, the magnetic pulses emitted from (say) a piece of iron as it is placed inside an increasing external field (see Fig. 3(a)).

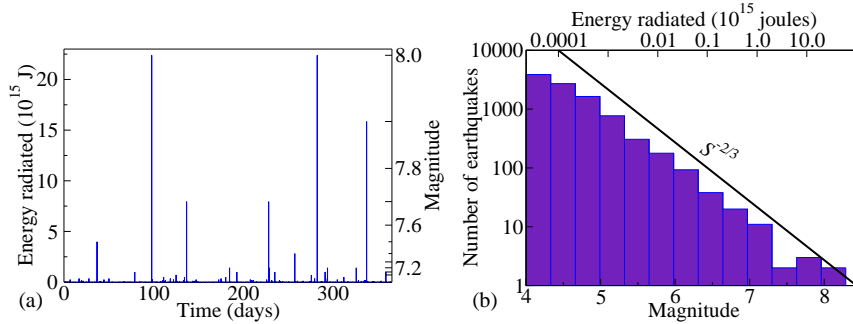


Fig. 1. **Earthquake sizes.** (a) Earthquake energy release versus time in 1995. There are only a few large earthquakes, and many small ones. This time series, when sped up, sounds like crackling noise [4]. (b) Histogram of the number of earthquakes in 1995 as a function of their magnitude M . Notice the logarithmic scales; the smallest earthquakes shown are a million times smaller and a thousand times more probable than the largest earthquakes. The fact that the earthquake size distribution is well described by a power is the Gutenberg–Richter law [5].

All of these systems share certain common features. They all have many more tiny events than large ones, typically with a *power-law* probability distribution (Figs 1(a), 2(a)). For example, the histogram of the number of earthquakes of a given size yields a straight line on a log–log plot (Figure 1b). This implies that the probability of a large earthquake goes as its size (energy radiated) to a power. The tearing avalanches in paper, dislocation avalanches in deformed ice, and rupture avalanches in steel all have power-law avalanche size distributions (Fig. 2(b)). Because crackling noise exhibits simple, emergent features (like these power law size distributions), it encourages us to expect that a theoretical understanding might be possible.

What features of, say, an earthquake fault do we expect to be important for such a theoretical model? If earthquake faults slipped only in large, snapping events we would expect to need to know the shape of the tectonic plates in order to describe them. If they slid more-or-less smoothly we anticipate that the nature of the internal rubble and dirt (fault gouge) would be important. But since earthquakes come in all sizes, we expect that neither the microscopic rock-scale nor the macroscopic continental-scale details can be crucial. What, then, is important to get right in a model?

An important hint is provided by looking at the dynamics of an individual avalanche. In many (but not all) systems exhibiting crackling noise, the avalanches themselves have complex, internal structures. Fig. 4 shows that the avalanches producing individual Barkhausen pulses in magnets proceed in an irregular, jerky

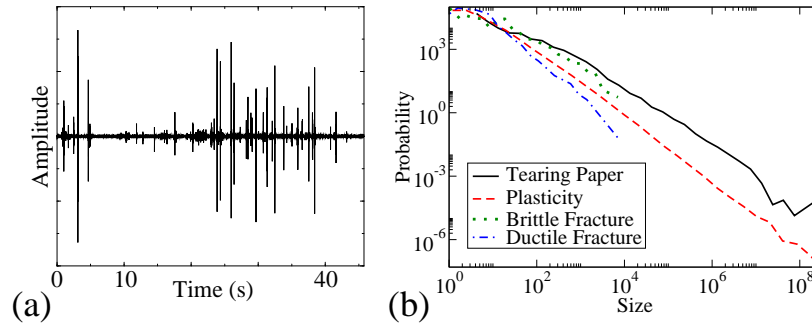


Fig. 2. (a) **Crackling noise in paper** $V(t)$ for multiple pulses, from [6]. Again, there are many small pulses, and only a few large events. (b) **Power laws** of event sizes for paper tearing [7], plastic flow in ice [8], and brittle and ductile fracture in steel [9].

fashion, almost stopping several times in between sub-avalanches. Fig. 5(a) shows that the spatial structure of an avalanche in a model magnet is also irregular. Both the time and spatial structures are *self-similar*; if we take one of the sub-avalanches and blow it up, it looks statistically much like the original avalanche. Large avalanches are built up from multiple, similar pieces, with each sub-avalanche triggering the next. It is the way in which one sub-avalanche triggers the next that is crucial for a theoretical model to get right.

Our focus in these lecture notes will be on understanding the emergent behavior in crackling noise (power laws and scaling functions) by exploring the consequences of this self-similar structure. In section 3, we illustrate the process by which models are designed and tested by experiments using Barkhausen noise. In section 4 we introduce the *renormalization group*, and use it to explain *universality* and self-similarity in these (and other) systems. In section 5 we use the renormalization group to explain the power laws characteristic of crackling noise, and also use it to derive the far more powerful *universal scaling functions*.

3. Hysteresis and Barkhausen noise in magnets

Microscopically, iron at room temperature is always magnetized; non-magnetic bulk iron is composed of tiny magnetic domains, whose north poles point in different directions giving a net zero magnetization. An external magnetic field, as in Fig. 3(a), will attract a piece of iron by temporarily moving the domain walls to enlarge the regions whose north poles are aligned towards the south pole

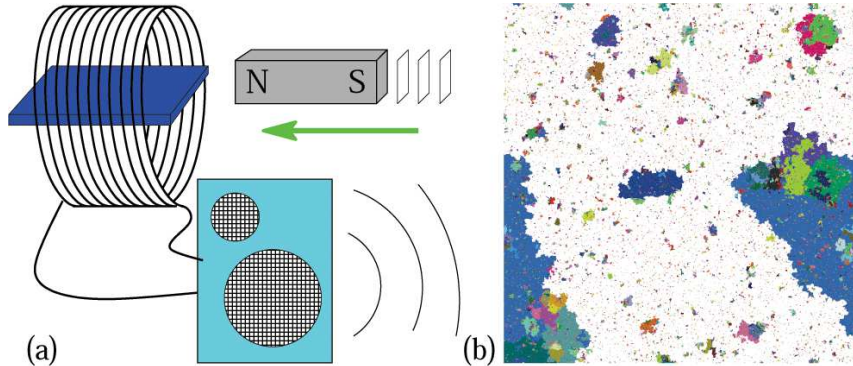


Fig. 3. (a) **Barkhausen noise experiment.** By increasing an external magnetic field $H(t)$ (bar magnet approaching), the magnetic domains in a slab of iron flip over to align with the external field. The resulting magnetic field jumps can be turned into an electrical signal with an inductive coil, and then listened to with an ordinary loudspeaker. Barkhausen noise from our computer experiments can be heard on the Internet [4]. (b) **Cross section of all avalanches** in a billion-domain simulation of our model for Barkhausen noise at the critical disorder [1]. The white background is the infinite, spanning avalanche.

of the external field. When the external field is removed, these domain walls do not completely return to their original positions, and the iron will end up partially magnetized; this history dependence is called *hysteresis*. The dependence of the magnetization of the iron M on the history of the external field H (the *hysteresis loop*) can have an interesting hierarchical structure of subloops (Fig. 6).

These hysteresis loops may look smooth, but when Fig. 6 is examined in detail we see that the magnetization grows in discrete jumps, or avalanches. These avalanches are the origin of magnetic Barkhausen noise. In section 3.1 we will develop a simple model for this Barkhausen noise. In section 3.2 we shall observe that our model, while capturing some of the right behavior, is not the correct model for real magnets, and introduce briefly more realistic models that do appear to capture rather precisely the correct behavior.¹

3.1. Dynamical Random-field Ising model

We introduce here a caricature of a magnetic material. We model the iron as a cubic grid of magnetic domains S_i , whose north pole is either pointing upward ($S_i = +1$) or downward ($S_i = -1$). The external field pushes on our domain with a force $H(t)$, which starts pointing down ($H(t=0) \ll 0$) and will increase

¹That is, we believe they are in the right *universality class*, section 4.1.

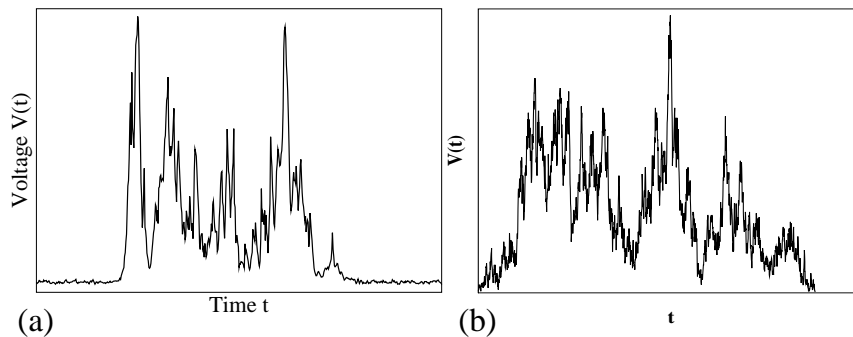


Fig. 4. **Internal avalanche time series** (a) during a single experimental Barkhausen noise pulse [19], and (b) during a single avalanche in a simulation of magnetic Barkhausen noise [1]. The experiment measures the voltage $V(t)$, which in this experiment measures the volume swept out per unit time by the moving magnetic domain wall; the simulation measures the number of domains flipped per unit time. In these two cases, the total area under the curve gives the size S of the avalanche. Notice how the avalanches almost stop several times; if the forcing were slightly smaller, the large avalanche would have broken up into two or three smaller ones. The fact that the forcing is just large enough to on average keep the avalanche growing is the cause of the self-similarity; a partial avalanche of size S will on average trigger one other of size S .

with time. Iron is magnetic because a domain has lower energy when it is magnetized in the same direction as its neighbors; the force on site i from the six neighboring domains S_j in our model is of strength $J \sum_j S_j$. Finally, we model the effects of impurities, randomness in the domain shapes, and other kinds of disorder by introducing a random field² h_i , different for each domain and chosen from a normal distribution with standard deviation $R \times J$. The net force on S_i is thus

$$F_i = H(t) + \sum_j JS_j + h_i, \quad (3.1)$$

corresponding to the energy function or Hamiltonian

$$\mathcal{H} = -J \sum_{\langle ij \rangle} S_i S_j - \sum_i (H(t) + h_i) S_i. \quad (3.2)$$

²Most disorder in magnets is not microscopically well described by random fields, but better modeled using random anisotropy or random bonds which do not break time-reversal invariance. For models of hysteresis, time-reversal symmetry is already broken by the external field, and all three types of randomness are probably in the same universality class. That is, random field models will have the same statistical behavior as more realistic models, at least for large avalanches and long times (see section 4.1).

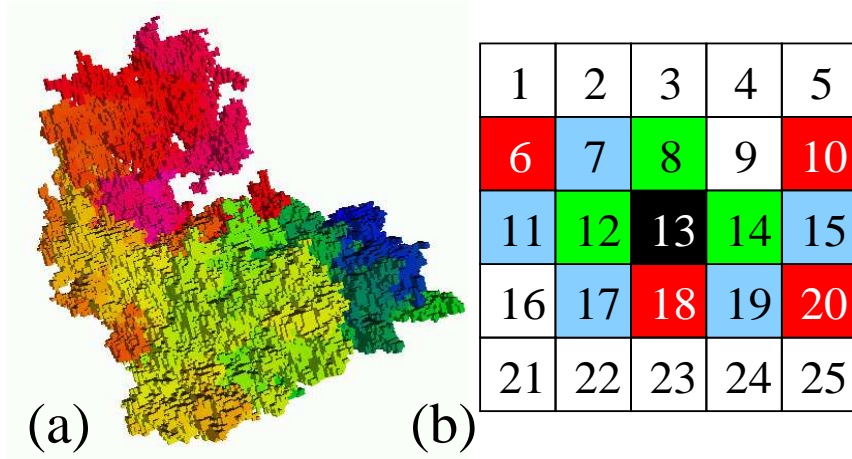


Fig. 5. (a) **Fractal spatial structure of an avalanche.** This moderate-sized avalanche contains 282,785 domains (or spins) [1]. The shading depicts the time evolution: the avalanche started in the dark region in the back, and the last domains to flip are in the upper, front region. The sharp changes in shading are real, and represent sub-avalanches separated by times where the avalanche almost stops (see Fig. 4). (b) **Avalanche propagation.** The avalanches in many models of crackling noise are first nucleated when the external stress induces a single site to transform. In this two-dimensional model, site #13 is the nucleating site which is first pushed over. The coupling between site #13 and its neighbors triggers some of them to flip (#4, 8, and 12), which in turn trigger another shell of neighbors (#15, 19, 7, 11, and 17), ending eventually in a final shell which happens not to trigger further sites (#6, 10, 18, and 20). The time series $V(t)$ plotted in figure 4(b) is just the number of domains flipped in shell # t for that avalanche.

This model is called the *random-field Ising model* (RFIM), and its thermal equilibrium properties have historically been studied as an archetypal disordered system with glassy dynamics. Here we ignore temperature (specializing to magnets where the thermal fluctuations are too small to de-pin the domain walls), and assume that each domain S_i reorients whenever its local field F_i changes sign, to minimize its energy.

In our model, there are two situations where a domain will flip. It may be induced to flip directly by a change in the external field $H(t)$, or it may be triggered to flip by the flipping of one of its neighboring domains. The first case corresponds to nucleating a new avalanche; the second propagates the avalanche outward from the triggering domain, see Fig. 5(b). We assume that the external field $H(t)$ changes slowly enough that each avalanche finishes (even ones which sweep over the entire magnet) before the field changes appreciably.

These avalanches can become enormous, as in Fig. 5(a). How can an avalanche

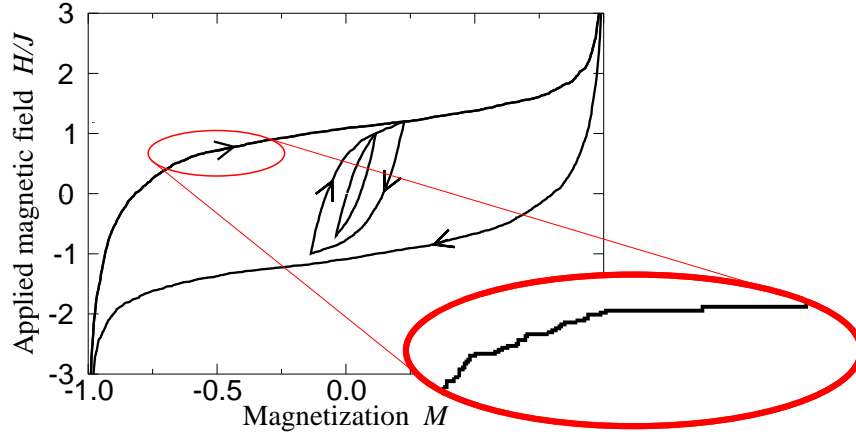


Fig. 6. **Hysteresis loop and subloops**: The magnetization in our model [20], as the external field H is ramped up and down. Our focus will primarily be on the upper, outer loop as the external field is ramped from $-\infty$ to ∞ . **Barkhausen jumps** (exploded region): The hysteresis loop appears smooth, but when examined in detail is composed of discrete, abrupt jumps in magnetization, corresponding to avalanches in the positions of the walls of the magnetic domains. This jerky magnetization is what emits *Barkhausen noise*.

grow to over 10^5 domains, but then halt? In our model, it happens only when the disorder R and the field $H(t)$ are near a *critical point* (Fig. 7). For large disorder compared to the coupling between domains $R \gg J \equiv 1$, each domain turns over almost independently (roughly when the external field $H(t)$ cancels the local random field h_i , with the alignment of the neighbors shifting the transition only slightly); all avalanches will be tiny. For small disorder compared to the coupling $R \ll J$, there will typically be one large avalanche that flips most of the domains in the sample. (The external field $H(t)$ needed to nucleate the first domain flip will be large, to counteract the field $-6J$ from the unflipped neighbors without substantial assistance from the random field; at this large external field most of the neighboring domains will be triggered, ... eventually flipping most of the domains in the entire system). There is a critical disorder R_c separating two qualitative regimes of behavior—a phase $R > R_c$ where all avalanches are small and a phase $R < R_c$ where one ‘infinite’ avalanche flips a finite fraction of all domains in the system (Fig. 7). Near³ R_c , a growing avalanche doesn’t know whether it should grow forever or halt while small, so a distribution of avalanches of all sizes might be expected— giving us crackling noise.

³One must also be near the field $H(t) = H_c$ where the infinite avalanche line ends.

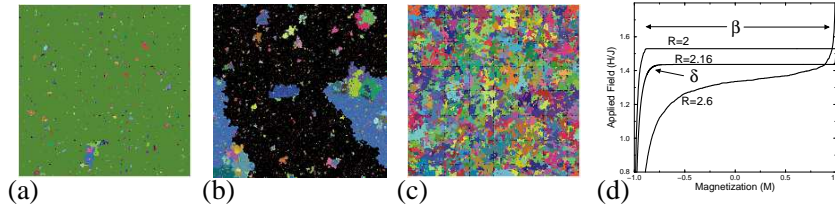


Fig. 7. Phase transition in hysteresis and avalanche model; (a) one enormous avalanche (background) for small disorder $R < R_c$, (b) avalanches at all scales at $R = R_c$ (c) many small avalanches for large disorder $R > R_c$. (d) The upper branch of the hysteresis loop develops a macroscopic jump in magnetization below R_c , whose size diverges as $\Delta M \propto (R - R_c)^\beta$; at $R = R_c$ the magnetization has a power-law singularity $M - M_c \sim (H - H_c)^{1/\delta}$.

3.2. Real Barkhausen noise

Is our model a correct description of Barkhausen noise in real magnets? Our model does capture the qualitative physics rather well; near R_c it exhibits crackling noise with a broad distribution of avalanche sizes (Fig. 3(b)), and the individual avalanches have the same kind of internal irregular dynamical structure as seen in real Barkhausen avalanches (Fig. 4).

However, when examined in detail we find that there are problems with the model. A typical problem might be that the theoretically predicted power-law is wrong (Fig. 8). The probability density $\mathcal{D}(S)$ of an avalanche of size S experimentally [21] decays as a power law $\mathcal{D}(S) \sim S^{-\tau}$, with values of the exponent that cluster around either $\tau = 1.27$ or $\tau = 1.5$. In our model at R_c and near H_c we find $\tau = 1.6 \pm 0.06$, which is marginally compatible with the data for the second group of samples (see Fig. 15(a)). If the power law were significantly different, our model would have been ruled out. We shall see in section 5 that the power laws are key *universal* predictions of the theory, and if they do not agree with the experiment then the theory is missing something crucial.

However, there are two other closely related avalanche models that describe the two groups of experiments well. One is a front propagation or fluid invasion model (which preceded ours [15, 22–24]), also usually written as a random-field Ising model but here starting with an existing front and allowing new avalanches only contiguous to previously flipped domains (water can invade new pores only next to currently wet pores). The front-propagation model does well in describing the dynamics and size distribution of the materials with $\tau \approx 1.27$. The other model can either be viewed as the motion of a flat domain wall [25, 26] or the mean-field limit of the random-field Ising model [27, 28]; it has a value $\tau = 3/2$ nicely describing the other class of materials. These models incorporate the long-

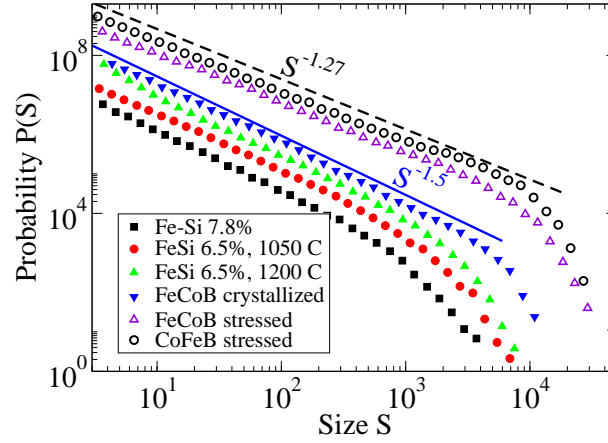


Fig. 8. **Avalanche size distributions** for magnetic Barkhausen noise in various materials, from [21]. The materials fall into two families, with power law exponent $D(S) \sim S^{-\tau}$ with $\tau \sim 1.5$ and $\tau \sim 1.27$. The cutoffs in the avalanche size distribution at large S are due to demagnetization effects, and scale as $S_{\max} k^{-1/\sigma_k}$ (section 5.1, Fig. 17).

range magnetic interactions between flipped domains, which experimentally produce demagnetizing fields that induce the magnetic domain wall to move rather rigidly.



Fig. 9. **Domain structure in a real magnet**, measured with a scanning electron microscope, digitally processed to detect edges. The horizontal lines are magnetic domain walls. Courtesy of K. Zaveta, from [29].

It is easy to measure the exponents of a power-law decay, but it is difficult to measure them well. We could argue that $\tau = 1.6$ is close enough to some of the experimental measurements that our model is not ruled out. But even a brief investigation of the qualitative behavior in these systems leads us to abandon hope. Fig. 9 shows the domain-wall structure in a real magnet. The domain walls

are indeed flat, and the way in which they advance (looking at animated versions of this figure, or observing directly through a microscope) is not by nucleating new walls, but by motion of existing boundaries.

4. Why Crackling Noise?

In this section we introduce *universality*, the *renormalization group*, and *self-similarity*. These three notions grew out of the theory of continuous phase transitions in thermal statistical mechanics, and are the basis of our understanding of a broad variety of systems, from quantum transitions (insulator to superconductor) to dynamical systems (the onset of chaos) [3, chapter 12]. We will illustrate and explain these three topics not only with our model for crackling noise in magnets, but also using classic problems in statistical mechanics—percolation and the liquid-gas transition. The renormalization group is our tool for understanding crackling noise.

4.1. Universality

Consider holding a sheet of paper by one edge, and sequentially punching holes of a fixed size at random positions. If we punch out only a few holes, the paper will remain intact, but if the density of holes approaches one the paper will fall apart into small shreds. There is a phase transition somewhere in between where the paper first ceases to hold together. This transition is called *percolation*.

Fig. 10 shows two somewhat different microscopic realizations of this problem. On the top we see a square mesh of bonds, where we remove all but a fraction p of the bonds. On the bottom we see a lattice of hexagonal regions punched out at random. Microscopically, these two processes seem completely different (left figures). But if we observe large simulations and examine them at long length scales, the two microscopic realizations yield statistically identical types of percolation clusters (right Figs 10).

Universality arises when the statistical morphology of a system at a phase transition is largely independent of the microscopic details of the system, depending only on the type (or *universality class*) of the transition. This should not come as a complete surprise; we describe most liquids with the same continuum laws (the Navier-Stokes equations) despite their different molecular makeups, with only the mass density and the viscosity depending on microscopic details. Similarly most solids obey elasticity theory on scales large compared to their constituent particles. For these phases we understand the material independence of the constituent equations by taking a continuum limit, assuming all behavior is slowly varying on the scale of the particles. At critical points, because our system is

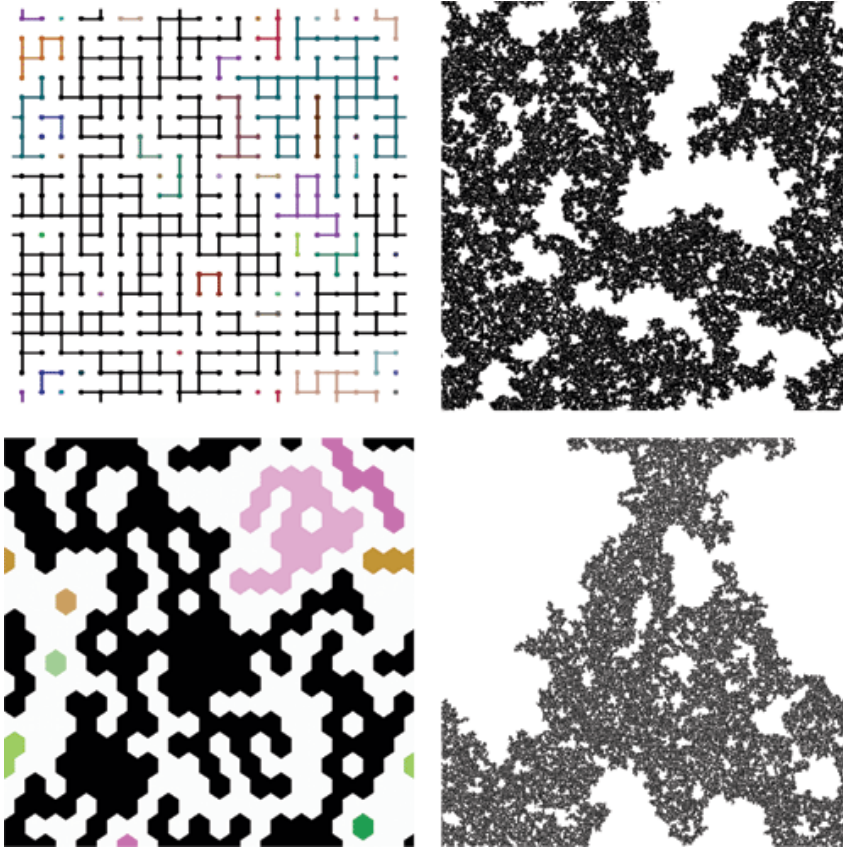


Fig. 10. **Universality in percolation.** Universality suggests that the entire morphology of the percolation cluster at p_c should be independent of microscopic details. On the top, we have bond percolation, where the bonds connecting nodes on a square lattice are occupied at random with probability p ; the top right shows the infinite cluster on a 1024×1024 lattice at the critical point. On the bottom, we have site percolation on a triangular lattice, where it is the hexagonal sites that are occupied. Even though the microscopic lattices and occupation rules are completely different, the resulting clusters look statistically identical at their critical points. (One should note that the site percolation cluster is slightly less dark. Universality holds up to overall scale changes, here up to a change in the density.)

rugged and complicated all the way down to the lattice scale, we will need a more sophisticated way of understanding universality (section 4.2).

Most thermal phase transitions are not continuous, and do not have structure on all scales. Water is water until it is heated past the boiling point, after which it abruptly turns to vapor (with a big drop in density ρ). Even boiling water, though, can show big fluctuations at high enough pressure. As we raise the pressure the boiling temperature gets larger and the density drop gets smaller, until at a certain pressure and temperature (P_c, T_c) the two densities become equal (to ρ_c). At this critical point the H₂O molecules do not know which phase they want to be in, and they show fluctuations on all scales.

Figure 11(a) shows that the approach to this critical point has universal features. If we divide the density by ρ_c and the temperature by T_c , many different liquids share the same ρ, T phase diagram,

$$\rho^{\text{Ar}}(T) = A\rho^{\text{CO}}(BT). \quad (4.1)$$

This is partly for mundane reasons; most of the molecules are roughly spherical, and have weak interactions.

But figure 11(b) shows the phase diagram of a completely different system, a magnet whose magnetization $M(T)$ vanishes as the temperature is raised past its T_c . The curve here does not agree with the curves in the liquid-gas collapse, but it can agree if we shear the axes slightly:

$$\rho^{\text{Ar}}(T) = A_1 M(BT) + A_2 + A_3 T. \quad (4.2)$$

Nature has decided that the ‘true’ natural vertical coordinate for the liquid-gas transition is not T but the line $T = (\rho - A_2)/A_3$. Careful experiments, measuring a wide variety of quantities, show that the liquid-gas transition and this type of magnet share many properties, except for smooth changes of coordinates like that in eq 4.2. Indeed, they share these properties also with a theoretical model—the (thermal, non-random, three-dimensional) Ising model. Universality not only tied disparate experiments together, it also allows our theories to work.

The agreement between Figs 11(a) and (b) may not seem so exciting; both are pretty smooth curves. But notice that they do not have parabolic tops (as one would expect from the maxima of a typical function). Careful measurements show that the magnet, the liquid-gas critical point, and the Ising model all vary as $(1 - T/T_c)^\beta$ with the same, probably irrational exponent β ; the best theoretical estimates have $\beta = 0.325 \pm 0.005$ [32, chapter 28]. This characteristic power law represents the effects of the large fluctuations at the critical points (the peaks of these graphs). Like the avalanche size distribution exponent τ , β is a *universal critical exponent* (section 5.1).

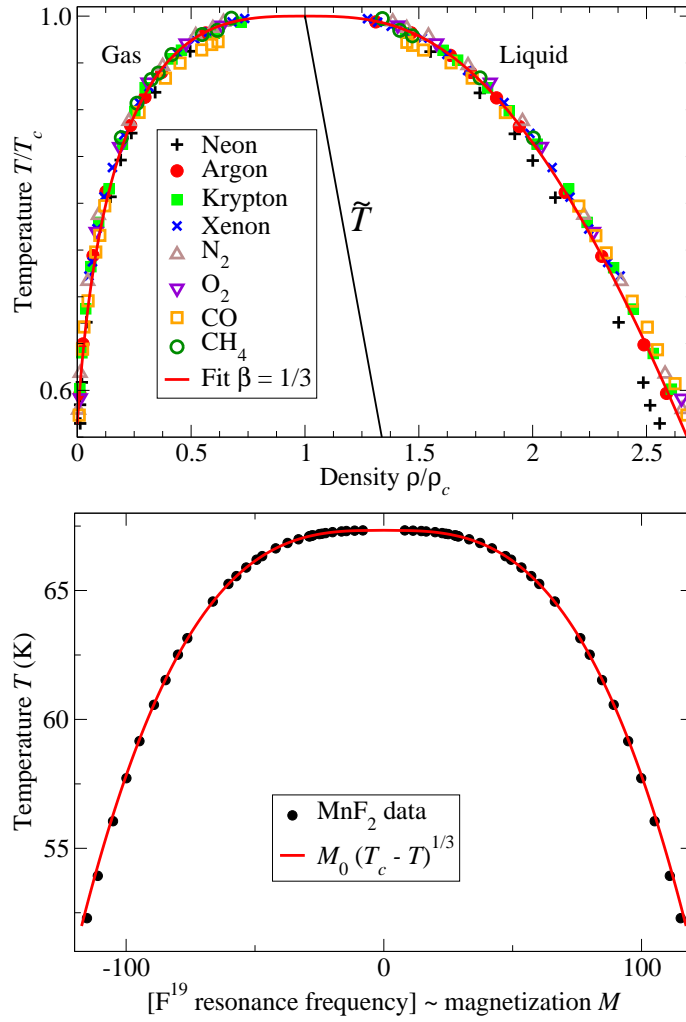


Fig. 11. **Universality.** (a) Universality at the liquid–gas critical point. The liquid–gas coexistence lines ($\rho(T)/\rho_c$ versus T/T_c) for a variety of atoms and small molecules, near their critical points (T_c, ρ_c) [30]. The gas phases lie on the upper left; the liquid phase region is to the upper right; densities in between will separate into a portion each of coexisting liquid and gas. The curve is a fit to the argon data, $\rho/\rho_c = 1 + s(1 - T/T_c) \pm \rho_0(1 - T/T_c)^\beta$ with $s = 0.75$, $\rho_0 = 1.75$, and $\beta = 1/3$ [30]. (b) Universality: ferromagnetic–paramagnetic critical point. Magnetization versus temperature for a uniaxial antiferromagnet MnF_2 [31]. The tilted line in (a) corresponds to the vertical axis in (b).

4.2. Renormalization group

Our explanation for universality, and our theoretical framework for studying crackling noise, is the *renormalization group*. The renormalization group starts with a remarkable abstraction: it works in an enormous ‘system space’. Different points in system space represent different materials under different experimental conditions, or different theoretical models with different interactions and evolution rules. For example, in Fig. 12(a) we consider the space of all possible models and experiments on hysteresis and avalanches, with a different dimension for each possible parameter (disorder R , coupling J , next-neighbor coupling, ...) and for each parameter in an experiment (chemical composition, annealing time, ...). Our theoretical model will traverse a line in this infinite-dimensional space as the disorder R is varied.

The renormalization group studies the way in which system space maps into itself under *coarse-graining*. The coarse-graining operation shrinks the system and removes microscopic degrees of freedom. Ignoring the microscopic degrees of freedom yields a new physical system with the same properties at long length scales, but with different (renormalized) values of the parameters. As an example, figure 13 shows a real-space renormalization-group ‘majority rule’ coarse-graining procedure applied to the Ising model. Many approximate methods have been devised to implement this coarse-graining operation (real-space, ϵ -expansions, Monte Carlo...) which we will not discuss here.

Under coarse-graining, we often find a fixed point S^* in system space. All of the systems that flow into this fixed point under coarse-graining will share the same long-wavelength properties, and will hence be in the same universality class.

Fig. 12(a) shows the case of a fixed point S^* with one unstable direction. Points deviating from S^* in this direction will flow away from it under coarse-graining. There is a surface C of points which do flow into the fixed point, which separates system space into two different phases (say, one with all small avalanches and one with one system-spanning, ‘infinite’ avalanche). The set C represents a universality class of systems at their critical points. Thus, fixed points with one unstable direction represent phase transitions.

Cases like the liquid-gas transition with two tuning parameters (T_c, ρ_c) determining the critical point will have two unstable directions. What happens when we have no unstable directions? The fixed-point S_a in Fig. 12(b) represents an entire region in system space sharing the same long-wavelength properties; it represents a *phase* of the system. Usually phases do not show structure on all scales, but some cases (like random walks) show this *generic scale invariance*.

Sometimes the external conditions acting on a system naturally drive it to stay at or near a critical point, allowing one to spontaneously observe fluctuations on

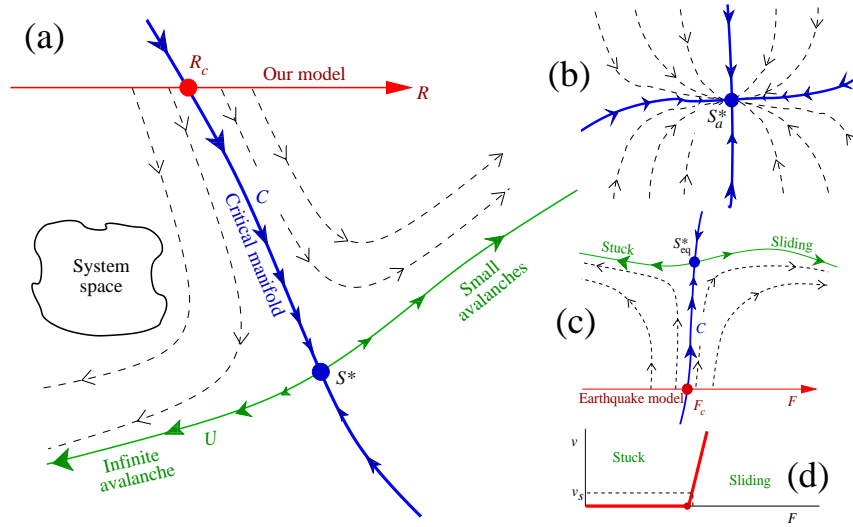


Fig. 12. **Renormalization–group flows** [1]. (a) **Flows describing a phase transition.** The renormalization–group uses coarse–graining to longer length scales to produce a mapping from the space of physical systems into itself. Consider the space of all possible systems exhibiting magnetic hysteresis (including, both real models and experimental systems). Each model can be coarse–grained, removing some fraction of the microscopic domains and introducing more complex dynamical rules so that the remaining domains still flip over at the same external fields. This defines a mapping of our space of models into itself. A fixed point S^* in this space will be self–similar: because it maps into itself upon coarse–graining, it must have the same behavior on different length scales. Points that flow into S^* under coarse–graining share this self–similar behavior on sufficiently long length scales: they all share the same *universality class*. (b) **Attracting fixed point** [1]. Often there will be fixed points that attract in all directions. These fixed points describe typical behavior: phases rather than phase transitions. Most phases are rather boring on long length scales. In more interesting cases, like random walks, systems can exhibit self–similarity and power laws without special tuning of parameters. This is called *generic scale invariance*. (c,d) **Flows for a front–propagation model** [1]. The front propagation model has a critical field F_c at which the front changes from a pinned to sliding state. (c) Coarse–graining defines a flow on the space of earthquake models. The critical manifold C , consisting of models which flow into S_{fp}^* , separating stuck faults from faults which slide forward with an average velocity $v(F)$. (d) The velocity varies with the external force F across the fault as a power law $v(F) \sim (F - F_c)^\beta$. Clever experiments, or long–range fields, can act to control not the external field, but the position: changing the front displacement slowly sets $v \approx 0$, thus self–tuning $F \approx F_c$. This is one example of *self–organized criticality*.

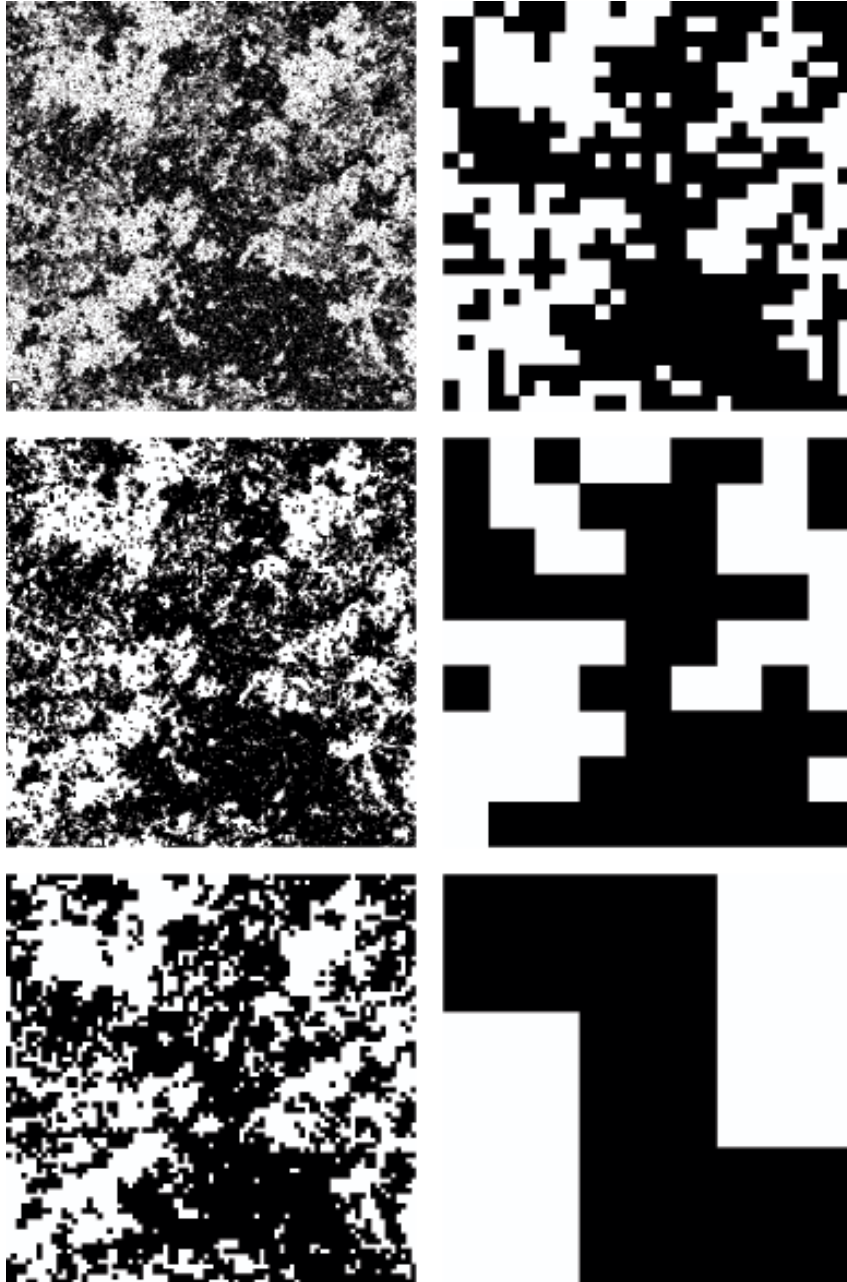


Fig. 13. **Ising model at T_c : coarse-graining.** Coarse-graining of a snapshot of the two-dimensional Ising model at its critical point. Each coarse-graining operation changes the length scale by a factor $B = 3$. Each coarse-grained spin points in the direction given by the majority of the nine fine-grained spins it replaces. This type of coarse-graining is the basic operation of the real-space renormalization group.

all scales. A good example is provided by certain models of earthquake fault dynamics. Fig. 12(c) schematically shows the renormalization-group flow for an earthquake model. It has a *depinning* fixed point representing the external force F across the fault at which the fault begins to slip; for $F > F_c$ the fault will slide with a velocity $v(F) \sim (F - F_c)^\beta$. Only near F_c will the system exhibit earthquakes of all sizes. Continental plates, however, do not impose constant forces on the faults between them; they impose a rather small constant velocity (on the order of centimeters per year, much slower than the typical fault speed during an earthquake). As illustrated in Fig. 12(d), this naturally sets the fault almost precisely at its critical point, tuning the system to its phase transition. This is called *self-organized criticality*.

In broad, the existence of fixed points under renormalization group coarse-graining is our fundamental explanation for universality. Real magnets, Ising models, and liquid-gas systems all apparently flow to the same fixed points under coarse graining, and hence show the same characteristic fluctuations and behaviors at long length scales.

5. Self-similarity and its consequences

The most striking feature of crackling noise and other critical systems is self-similarity, or scale invariance. We can see this vividly in the patterns observed in the Ising model (upper left, Fig. 13), percolation (Fig. 10), and our RFIM for crackling noise (Fig. 5a). Each shows roughness, irregularities, and holes on all scales at the critical point. This roughness and fractal-looking structure stems at root from a hidden symmetry in the problem: these systems are (statistically) invariant under a change in *length scale*.

Consider Fig. 14, depicting the self-similarity of the avalanches in our RFIM simulation at the critical disorder. The upper-right figure shows the entire system, and each succeeding picture zooms in by another factor of two. Each zoomed-in picture has a black ‘background’ showing the largest avalanche spanning the entire system, and a variety of smaller avalanches of various sizes. If you blur your eyes a bit, the figures should look roughly alike. This rescaling and blurring process is the renormalization-group coarse-graining transformation.

How does the renormalization group explain self-similarity? The fixed point S^* under the renormalization group is the same after coarse-graining (that’s what it means to be a fixed point). Any other system that flows to S^* under coarse graining will also look self-similar (except on the microscopic scales that are removed in the first few steps of coarse-graining, during the flow to S^*). Hence systems at their critical points naturally exhibit self-similarity.

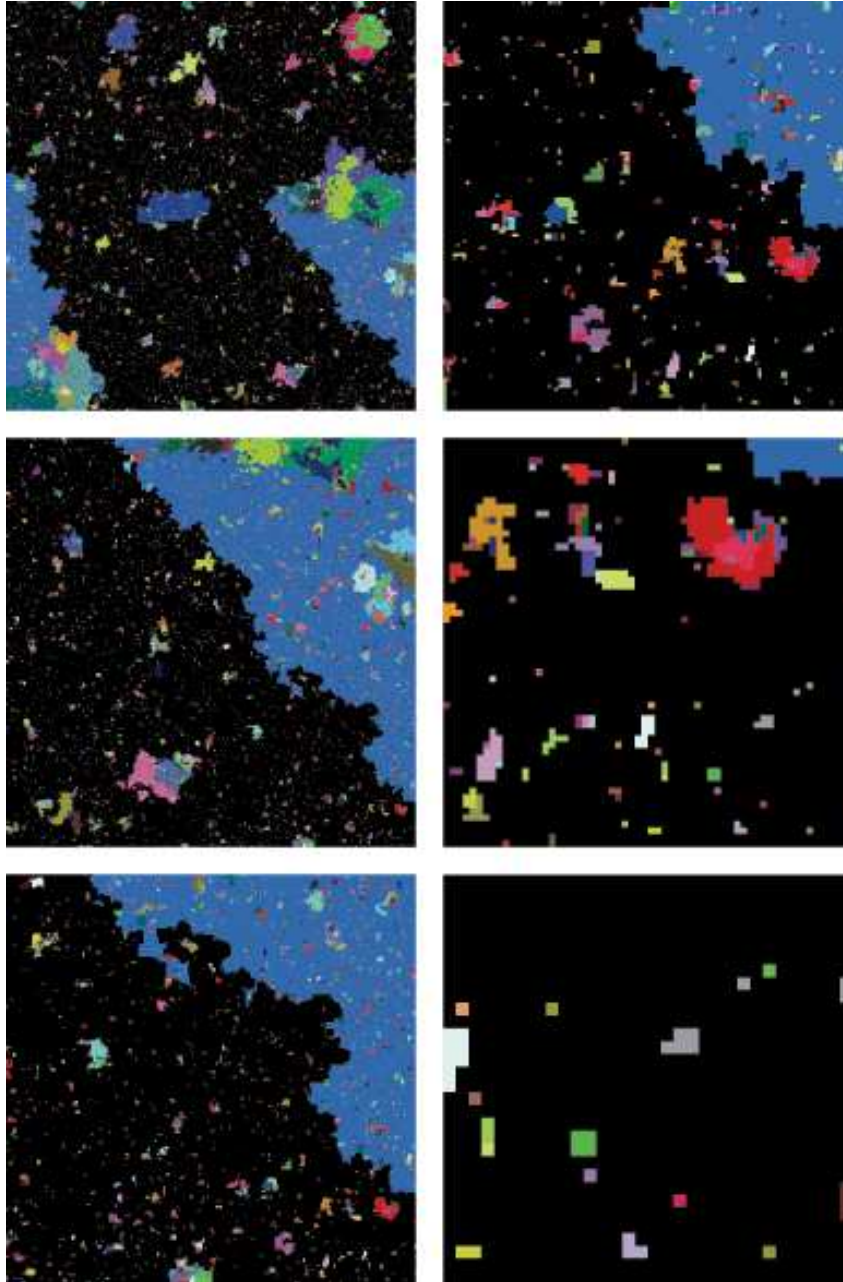


Fig. 14. **Avalanches: scale invariance.** Magnifications of a cross-section of all the avalanches in a run of our hysteresis model each one the lower right-hand quarter of the previous. The system started with a billion domains (1000^3). Each avalanche is shown in a different shade. Again, the larger scales look statistically the same.

This scale invariance can be thought of as an emergent symmetry, invariance under changes of length scale. In a system invariant under a translational symmetry, the expectation of any function of two positions x_1 and x_2 can be written in terms of the separation between the two points, $\langle g(x_1, x_2) \rangle = \mathcal{G}(x_2 - x_1)$. In just the same way, scale invariance will allow us to write functions of N variables in terms of *scaling functions* of $N - 1$ variables—except that these scaling functions are typically multiplied by power laws in one of these variables.

5.1. Power laws

Let us begin with the case of functions of one variable. Consider the avalanche size distribution $D(S)$ for a model, say the real earthquakes in Fig. 1(a), or our model for hysteresis at its critical point. Imagine taking the same system, but increasing the units of length with which we measure the system—stepping back, blurring our eyes, and looking at the system on a coarse-grained level. Let us multiply the spacing between markings on our rulers by a small amount $B = (1 + \epsilon)$. After coarsening, any length scales in the problem (like the spatial extent L of a particular avalanche) will be divided by B . The avalanche size (volume) S after coarse-graining will also be smaller by some factor⁴ $C = (1 + c\epsilon)$. Finally, the overall scale of $D(S)$ after coarse-graining will be changed by some factor $A = 1 + a\epsilon$.⁵ Hence under the coarse-graining we have

$$\begin{aligned} L' &= L/B = L/(1 + \epsilon), \\ S' &= S/C = S/(1 + c\epsilon), \\ D' &= AD = D(1 + a\epsilon). \end{aligned} \tag{5.1}$$

Now the probability that the coarse-grained system has an avalanche of size S' is given by the rescaled probability that the original system had an avalanche of size $S = (1 + c\epsilon)S'$:

$$D'(S') = AD(CS') = (1 + a\epsilon)D((1 + c\epsilon)S'). \tag{5.2}$$

Here $D'(S')$ is the distribution measured with the new ruler: a smaller avalanche with a larger probability density. Because we are at a self-similar critical point, the coarse-grained distribution $D'(S')$ should equal $D(S')$. Making ϵ infinitesi-

⁴If the size of the avalanche were the cube of its length, then c would equal three since $(1 + \epsilon)^3 = 1 + 3\epsilon + O(\epsilon^2)$. In general, c is the *fractal dimension* of the avalanche.

⁵The same avalanches occur independent of your measuring instruments! But the probability $D(S)$ changes, because the *fraction* of large avalanches depends upon how many small avalanches you measure, and because the fraction per unit S changes as the scale of S changes.

mal leads us to a differential equation:

$$\begin{aligned} D(S') &= D'(S') = (1 + a\epsilon)D((1 + c\epsilon)S'), \\ 0 &= a\epsilon D + c\epsilon S' \frac{D}{S}, \\ \frac{D}{S} &= -\frac{aD}{cS}, \end{aligned} \tag{5.3}$$

which has the general solution

$$D = D_0 S^{-a/c}. \tag{5.4}$$

Because the properties shared in a universality class only hold up to over-all scales, the constant D_0 is system dependent. However, the exponents a , c , and a/c are *universal*—independent of experiment (within the universality class). Some of these exponents have standard names: the exponent c giving the fractal dimension of the avalanche is usually called d_f or $1/\sigma\nu$. The exponent a/c giving the size distribution law is called τ in percolation and in most models of avalanches in magnets⁶ and is related to the Gutenberg–Richter exponent for earthquakes⁷ (Fig. 1(b)). Most measured quantities depending on one variable will have similar power-law singularities at the critical point. For example, the distribution of avalanche durations and peak heights also have power-law forms. This is because power laws are the only self-similar functions. If $f(x) = x^{-\alpha}$, then on a new scale multiplying x by B , $f(Bx) = B^{-\alpha}x^{-\alpha} \propto f(x)$.

Crackling noise involves several power laws. We've seen that the probability of having an avalanche of size S goes as $S^{-\tau}$. In our RFIM model for hysteresis, if one is at a distance $R - R_c$ from the critical point, there will be a cutoff in the avalanche size distribution. The typical largest spatial extent L of an avalanche is called the *correlation length* ξ , which scales as $\xi \sim (R - R_c)^{-\nu}$. The cutoff in the avalanche size S scales as $(R - R_c)^{-\sigma}$ (Fig 17). In other models, demagnetization effects (parameterized by k) lead to cutoffs in the avalanche size distribution [21], with analogous critical exponents ν_k and σ_k . The size and spatial extent of the avalanches are related to one another by a power law $S \sim L^{d_f}$, where $d_f = 1/\sigma\nu$ is called the *fractal dimension*. The duration of an avalanche goes as L^z . The probability of having an avalanche of duration T goes as $T^{-\alpha}$, where $\alpha = (\tau -$

⁶ In our RFIM for hysteresis, we use τ to denote the avalanche size law at the critical field and disorder ($D(S, R_c, H_c) \sim S^{-\tau}$); integrated over the hysteresis loop $D_{\text{int}} \propto S^{-\bar{\tau}}$ with $\bar{\tau} = \tau + \sigma\beta\delta$.

⁷We must not pretend that we have found the final explanation for the Gutenberg–Richter law. There are many different models that give exponents $\approx 2/3$, but it remains controversial which of these, if any, are correct for real-world earthquakes.

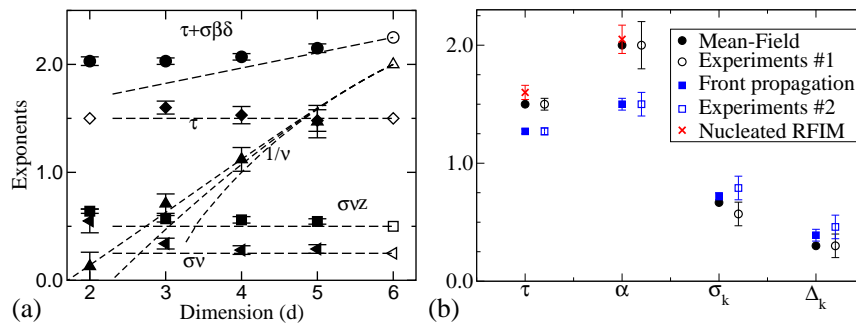


Fig. 15. (a) **Universal Critical Exponents in Various Spatial Dimensions.** [1] We test our ϵ -expansion predictions [34] by measuring the various critical exponents numerically in up to five spatial dimensions [35, 36]. The various exponents are described in the text. All of the exponents are calculated only to linear order in ϵ , except for the correlation length exponent ν , where we use results from other models. The agreement even in three dimensions is remarkably good, considering that we're expanding in $6 - D$ where $D = 3$! (b) **Universal Critical Exponents vs. Experiment** [21]. The exponent τ gives the probability density $\sim S^{-\tau}$ of having an avalanche of size S , α gives the probability density $\sim T^{-\alpha}$ of having an avalanche of duration T , and the exponents σ_k and Δ_k describe the cutoff in the avalanche sizes and durations, respectively, due to the demagnetizing field (see [21]). The experimental samples group naturally into two groups, described by the mean-field and front-propagation universality classes; none appear to be described well by our nucleated RFIM.

$1)/\sigma\nu z + 1$.⁸ In our RFIM, the jump in magnetization goes as $(R - R_c)^\beta$, and at R_c the magnetization $(M - M_c) \sim (H - H_c)^{1/\delta}$ (Fig. 7(d)).

To specialists in critical phenomena, these exponents are central; whole conversations often rotate around various combinations of Greek letters. We know how to calculate critical exponents from various analytical approaches; given an implementation of the renormalization group they can be derived from the eigenvalues of the linearization of the renormalization-group flow around the fixed-point S^* in Fig. 12. Figure 15(a) shows our numerical estimates for several critical exponents of the RFIM model for Barkhausen noise [35, 36], together with our $6 - \epsilon$ expansions results [34, 37]. Of course, the challenge is not to get analytical work to agree with numerics: it is to get theory to agree with experiment. Figure 15(b) compares recent Barkhausen experimental measurements of the critical exponents to values from the three theoretical models.

⁸Notice that we can write d_f and α in terms of the other exponents. These are *exponent relations*; all of the exponents can typically be written in terms of two or three basic ones. We shall derive some exponent relations in section 5.2.

5.2. Scaling functions

Critical exponents are not everything, however. Many other scaling predictions are easily extracted from numerical simulations, even if they are inconvenient to calculate analytically. (Universality should extend even to those properties that we have not been able to write formulæ for.) In particular, there are an abundance of functions of two or more variables that one can measure, which are predicted to take universal *scaling forms*.

5.2.1. Average pulse shape

For example, let us consider the time history $V(t)$ of the avalanches (Fig. 4). Each avalanche has large fluctuations, but one can average over many avalanches to get a typical shape. Averaging $V(t)$ together for large and small avalanches would seem silly, since only the large avalanches will last long enough to contribute at late times. The experimentalists originally addressed this issue [40] by rescaling the voltages of each avalanche by the peak voltage and the time by the duration, and then averaging these rescaled curves (dark circles in Fig. 16b). But there are so many more small avalanches than large ones that it seems more sensible to study them separately.

Consider the average voltage $\bar{V}(T, t)$ over all avalanches of duration T . Universality suggests that this average should be the same for all experiments and (correct) theories, apart from an overall shift in time and voltage scales:

$$\bar{V}_{\text{exp}}(T, t) = A\bar{V}_{\text{th}}(T/B, t/B). \quad (5.5)$$

Comparing systems with a shifted time scale becomes simpler if we change variables; let $v(T, t/T) = \bar{V}(T, t)$. Now, as we did for the avalanche size distribution in section 5.1, let us compare a system with itself, after coarse-graining by a small factor $B = 1/(1 - \epsilon)$:

$$v(T, t/T) = Av(T/B, t/T) = (1 + a)v((1 - \epsilon)T, t/T). \quad (5.6)$$

Again, making ϵ small we find $av = T \partial v / \partial T$, with solution $v(T, t/T) = v_0(T)T^a$. Here the integration constant v_0 will now depend on t/T , so we arrive at the scaling form

$$\bar{V}(T, t) = T^a \mathcal{V}(t/T) \quad (5.7)$$

where the scaling function $\mathcal{V} \equiv v_0$ (up to an overall constant factor) is a universal prediction of the theory.

Can we write the exponent a in terms of the exponents we already know? Since the size of an avalanche is defined as the integral of $V(t)$, we can use

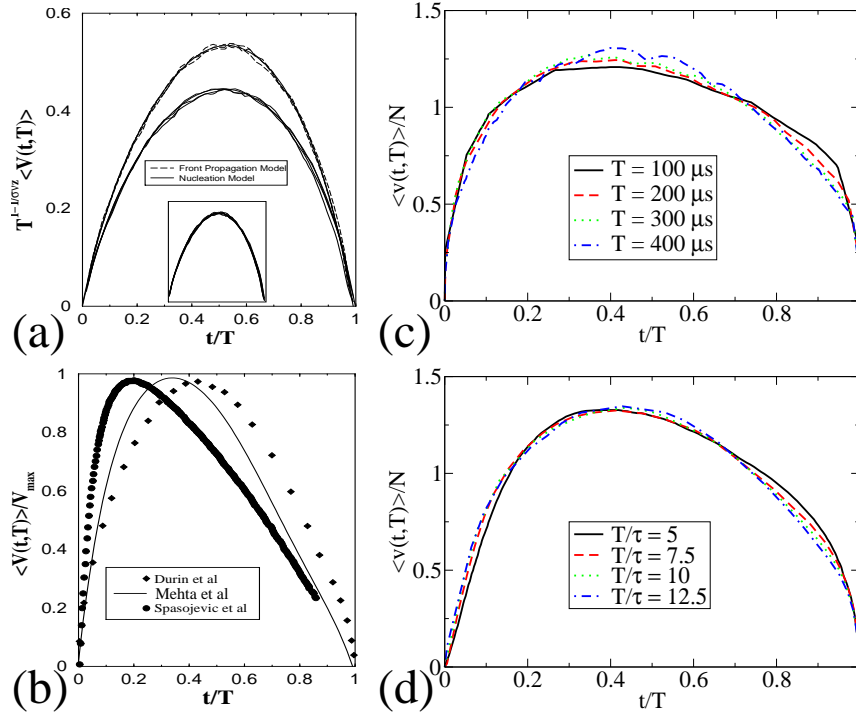


Fig. 16. (a) **Theoretical average pulse shape scaling functions** for our nucleated model and the front propagation model [38]. The overall height is non-universal; the two curves are otherwise extremely similar. The front propagation model has $1/\sigma\nu z = 1.72 \pm 0.03$ in this collapse; our nucleation model has $1/\sigma\nu z = 1.75 \pm 0.03$ (there is no reason to believe these two should agree). The inset shows the two curves rescaled to the same height (the overall height is a non-universal feature): they are quantitatively different, but far more similar to one another than either is to the experimental curves in part (b). (b) **Comparison of experimental average pulse shapes** for fixed pulse duration, as measured by three different groups [21, 38–40]. Notice that both theory curves are much more symmetric than those of the experiments. Notice also that the three experiments do not agree. This was a serious challenge to our ideas about the universality of the dynamics of crackling noise [1]. (c) **Pulse shape asymmetry experiment** [19]. Careful experiments show a weak but systematic duration dependence in the collapse of the average Barkhausen pulse shape. The longer pulses (larger avalanches) are systematically more symmetric (approaching the theoretical prediction). (d) **Pulse shape asymmetry theory** [19]. Incorporating the time-retardation effects of eddy currents into the theoretical model produces a similar systematic effect. The non-universal effects of eddy currents are in principle irrelevant for extremely large avalanches.

the scaling relation (eq 5.7) to write an expression for the average size of an avalanche of duration T ,

$$\bar{S}(T) = \int \bar{V}(t, T) \dagger = \int T^a \mathcal{V}(t/T) \dagger \sim T^{a+1}. \quad (5.8)$$

We also know that avalanches have fractal dimension $d_f = 1/\sigma\nu$, so $S \sim L^{1/\sigma\nu}$, and that the duration of an avalanche of size L goes as $T \sim L^z$. Hence $\bar{S}(T) \sim T^{1/\sigma\nu z} \sim T^{a+1}$, and $a = 1/\sigma\nu z - 1$. This is an example of an *exponent relation*.

Can we use the experimental pulse shape to figure out which theory is correct? Fig. 16(a) shows a *scaling collapse* of the pulse shapes for our RFIM and the front propagation model. The scaling collapse tests the scaling form eq 5.7 by attempting to plot the scaling function $\mathcal{V}(t/T) = T^{-a}V(t, T)$ for multiple durations T on the same plot. The two theoretical pulse shapes look remarkably similar to one another, and almost perfectly time-reversal symmetric. The mean-field model also is time-reversal symmetric.⁹ Thus none of the theories describe the strongly skewed experimental data (Fig. 16). Indeed, the experiments did not even agree with one another, calling into question whether universality holds for the dynamical properties.

This was recognized as a serious challenge to our whole theoretical picture [1, 38, 43]. An elegant, convincing physical explanation was developed by Colaioni *et al.* [44], who attribute the asymmetry to eddy currents, whose slow decay lead to a time-dependent damping of the domain wall mobility. Incorporating these eddy current effects into the model leads to a clear correspondence between their eddy-current theory and experiment, see Fig. 16(c,d). In those figures, notice that the scaling ‘collapses’ are imperfect, becoming more symmetric for avalanches of longer durations. These eddy-current effects are theoretically *irrelevant* perturbations; under coarse-graining, they disappear. So, the original models are in principle correct,¹⁰ but only for avalanches far larger and longer-lasting than those actually seen in the experiments.

5.2.2. Avalanche size distribution

Finally, let us conclude by analyzing the avalanche size distribution in our RFIM for hysteresis. The avalanche size distribution not only connects directly to many of the experiments (Fig. 8), it also involves a non-obvious example of a *scaling*

⁹The mean-field model apparently has a scaling function which is a perfect inverted parabola [41]. The (otherwise similar) rigid-domain-wall model, interestingly, has a different average pulse shape, that of one lobe of a sinusoid [42, eq. 3.102].

¹⁰One might wonder how the original models do so well for the avalanche size distributions and other properties, when they have such problems with the pulse shape. In models which obey *no passing* [45, 46], the domains flipped in an avalanche are independent of the dynamics; eddy currents in these models won’t change the shapes and sizes of the avalanches.

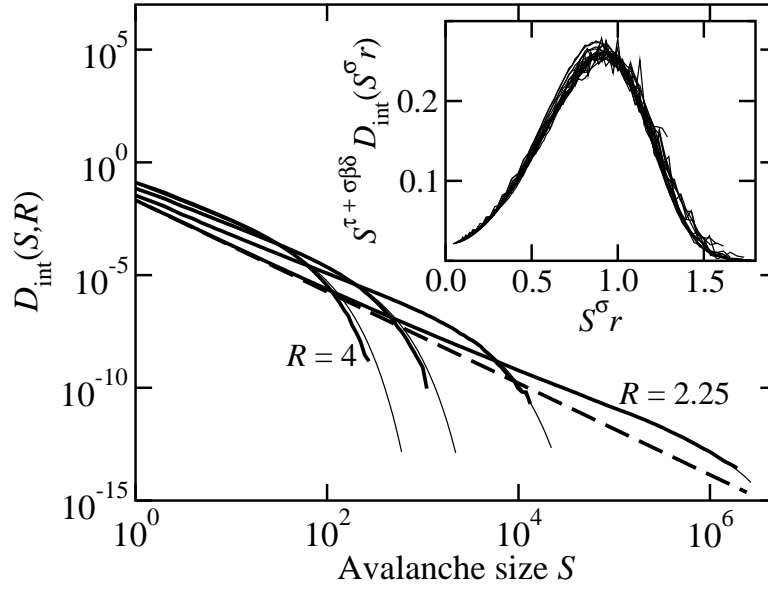


Fig. 17. **Avalanche size distribution.** The distribution of avalanche sizes in our model for hysteresis. Notice the logarithmic scales.¹² (i) Although only at $R_c \approx 2.16$ do we get a pure power law (dashed line, $D(S) \propto S^{-\bar{\tau}}$), we have large avalanches with hundreds of domains even a factor of two away from the critical point, and six orders of magnitude of scaling at 5% above R_c . (ii) The curves have the wrong slope except very close to the critical point. Be warned that a power law over two decades (although often publishable [47]) may not yield a reliable exponent. (iii) The scaling curves (thin lines) work well even far from R_c . Inset: We plot $D(S)/S^{-\bar{\tau}}$ versus $S^\sigma(R - R_c)/R$ to extract the universal scaling curve $\mathcal{D}(X)$ (eqn 5.15). (We use the exponent relation $\bar{\tau} = \tau + \sigma\beta\delta$ without deriving it; see footnote 6 on page 24.) Varying the critical exponents and R_c to get a good collapse allows us to measure the exponents far from R_c , where power-law fits are still unreliable.

variable). Fig. 17 shows the distribution of avalanche sizes $D_{\text{int}}(S, R)$ for different disorders $R > R_c$, integrated over the entire hysteresis loop (Fig. 6). We observe a power-law distribution near $R = R_c \sim 2.16$, that is cut off at smaller and smaller avalanches as we move away from R_c .¹³

Let us derive the scaling form for $D_{\text{int}}(S, R)$. By using scale invariance, we will be able to write this function of two variables as a power of one of the variables times a universal, one-variable function of a combined scaling variable. From our treatment at R_c (eqns 5.1) we know that

$$\begin{aligned} S' &= S / (1 + c\epsilon), \\ D' &= D (1 + a\epsilon). \end{aligned} \quad (5.9)$$

A system at $R = R_c + r$ after coarse-graining will have all of its avalanches reduced in size, and hence will appear similar to a system further from the critical disorder (where the cutoff in the avalanche size distribution is smaller, Fig. 7), say at $R = R_c + Er = R_c + (1 + e\epsilon)r$. Hence

$$\begin{aligned} D(S', R_c + Er) &= D'(S', R_c + r) = AD(CS', R_c + r), \\ D(S', R_c + (1 + e\epsilon)r) &= (1 + a\epsilon) D((1 + c\epsilon)S', R_c + r). \end{aligned} \quad (5.10)$$

To facilitate deriving the scaling form for multiparameter functions, it is helpful to change coordinates so that all but one variable remains unchanged under coarse-graining (the scaling variables). In the average pulse shape of section 5.2.1, the time t and the duration T change in the same way under coarse-graining, so the ratio was a scaling variable. For the avalanche size distribution, consider the combination $X = S^{e/c}r$. After coarse-graining $S' = S/C$ and shifting to the higher disorder $r' = Er$ this combination is unchanged:

$$\begin{aligned} X' &= S'^{e/c}r' = (S/C)^{e/c}(Er) = (S/(1 + c\epsilon))^{e/c}((1 + e\epsilon)r) \\ &= S^{e/c}r \left(\frac{1 + e\epsilon}{(1 + c\epsilon)^{e/c}} \right) = S^{e/c}r + O(\epsilon^2) = X + O(\epsilon^2). \end{aligned} \quad (5.11)$$

Let $\bar{D}(S, S^{e/c}R) = D(S, R)$ be the size distribution in terms of the variables S and X . Then \bar{D} coarse-grains much like a function of one variable, since X stays fixed. Equation 5.10 now becomes

$$\bar{D}(S', X') = \bar{D}(S', X) = (1 + a\epsilon) \bar{D}((1 + c\epsilon)S', X), \quad (5.12)$$

so

$$a\bar{D} = -cS' \frac{\partial \bar{D}}{\partial S'} \quad (5.13)$$

¹³This cutoff is the one described in section 5.1, scaling as $(R - R_c)^{-\sigma}$.

and hence

$$\bar{D}(S, X) = S^{-a/c} = S^{-\bar{\tau}}\mathcal{D}(X) \quad (5.14)$$

with the universal *scaling function* $\mathcal{D}(X)$. Rewriting things in terms of the original variables and the traditional Greek names for the scaling exponents ($c = 1/\sigma\nu$, $a = \bar{\tau}/\sigma\nu$, and $e = 1/\nu$), we find the scaling form for the avalanche size distribution:

$$D(S, R) \propto S^{-\bar{\tau}}\mathcal{D}(S^\sigma(R - R_c)). \quad (5.15)$$

We can use a *scaling collapse* of the experimental or numerical data to extract this universal function, by plotting $D/S^{-\bar{\tau}}$ against $X = S^\sigma(R - R_c)$; the inset of Fig. 17 shows this scaling collapse.

In broad terms, most properties that involve large scales of length and time at a critical point will have universal scaling forms; any N variable function will be writable in terms of a power law times a universal function of $N - 1$ variables, $F(x, y, z) \sim z^{-\alpha}\mathcal{F}(x/z^\beta, y/z^\gamma)$. The deep significance of the renormalization-group predictions are only feebly illustrated by the power-laws most commonly studied. The universal scaling functions, and other morphological self-similar features are the best ways to measure the critical exponents, the sharpest tests for the correctness of theoretical models, and provide the richest and most complete description of the complex behavior observed in these systems.

References

- [1] J. P. Sethna, K. A. Dahmen, and C. R. Myers. Crackling noise. *Nature*, 410:242, 2001.
- [2] James P. Sethna, Karin A. Dahmen, and Olga Perković. Random-field models of hysteresis, <http://arxiv.org/abs/cond-mat/0406320>. In *The Science of Hysteresis, Vol. II*, pages 107–179. Academic Press, 2006.
- [3] James P. Sethna. *Statistical Mechanics: Entropy, Order Parameters, and Complexity*, <http://www.physics.cornell.edu/sethna/StatMech/>. Oxford University Press, Oxford, 2006.
- [4] M. C. Kuntz, P. Houle, and J. P. Sethna. Crackling noise. sims.cornell.edu/, 1998.
- [5] B. Gutenberg and C. F. Richter. *Seismicity of the Earth and Associated Phenomena*. Princeton University, Princeton, NJ, 1954.
- [6] P. A. Houle and J. P. Sethna. Acoustic emission from crumpling paper. *Physical Review E*, 54:278, 1996.
- [7] L. I. Salminen, A. I. Tolvanen, and M. J. Alava. Acoustic emission from paper fracture. *Phys. Rev. Lett.*, 89:185503, 2002.
- [8] M. Carmen Miguel, A. Vespignani, S. Zapperi, J. Weiss, and J.-R. Grasso. Intermittent dislocation flow in viscoplastic deformation. *Nature*, 410:667, 2001.
- [9] F. Kun, Gy. B. Lenkey, N. Takács, and D. L. Beke. Structure of magnetic noise in dynamic fracture. *Phys. Rev. Lett.*, 93:227204, 2004.
- [10] E.M. Kramer and A.E. Lobkovsky. Universal power law in the noise from a crumpled elastic sheet. *Phys. Rev. E*, 53:1465–1469, 1996.

- [11] L. C. Krysac and J. D. Maynard. Evidence for the role of propagating stress waves during fracture. *Phys. Rev. Lett.*, 81:4428–31, 1998.
- [12] Knut Jørgen Måløy, Stéphane Santucci, Jean Schmittbuhl, and Renaud Toussaint. Local waiting time fluctuations along a randomly pinned crack front. *Phys. Rev. Lett.*, 96:045501, 2006.
- [13] S. Tewari, D. Schiemann, D.J. Durian, C.M. Knobler, S.A. Langer, and A.J. Liu. Statistics of shear-induced rearrangements in a two-dimensional model foam. *Phys. Rev. E*, 60:4385–4396, 1999.
- [14] N. Vandewalle, J.F. Lentz, S. Dorbolo, and F. Brisbois. Avalanches of popping bubbles in collapsing foams. *Phys. Rev. Lett.*, 86:179, 2001.
- [15] M. Cieplak and M.O. Robbins. Dynamical transition in quasistatic fluid invasion in porous media. *Phys. Rev. Lett.*, 60:2042–2045, 1988.
- [16] O. Narayan and D.S. Fisher. Threshold critical dynamics of driven interfaces in random media. *Phys. Rev. B*, 48:7030–42, 1993.
- [17] Michael D. Uchic, Dennis M. Dimiduk, Jeffrey N. Florando, and William D. Nix. Sample dimensions influence strength and crystal plasticity. *Science*, 305:986–9, 2004.
- [18] Dennis M. Dimiduk, Chris Woodward, Richard LeSar, and Michael D. Uchic. Scale-free intermittent flow in crystal plasticity. *Science*, 312:1188–90, 2006.
- [19] Stefano Zapperi, Claudio Castellano, Francesca Colaiori, and Gianfranco Durin. Signature of effective mass in crackling-noise asymmetry. *Nature Physics*, 1:46–9, 2005.
- [20] James P. Sethna, Karin Dahmen, Sivan Kartha, James A. Krumhansl, Bruce W. Roberts, and Joel D. Shore. Hysteresis and hierarchies: Dynamics of disorder-driven first-order phase transformations. *Physical Review Letters*, 70:3347–50, 1993.
- [21] G. Durin and S. Zapperi. Scaling exponents for barkhausen avalanches in polycrystalline and amorphous ferromagnets. *Phys. Rev. Lett.*, 84:4705–4708, 2000.
- [22] H. Ji and M. O. Robbins. Percolative, self-affine, and faceted domain growth in random 3-dimensional magnets. *Phys. Rev. B*, 46:14519, 1992.
- [23] O. Narayan. Self-similar barkhausen noise in magnetic domain wall motion. *Phys. Rev. Lett.*, 77:3855–3857, 1996.
- [24] B. Koiller and M. O. Robbins. Morphology transitions in three-dimensional domain growth with gaussian random fields. *Phys. Rev. B*, 62:5771–5778, 2000. and references therein.
- [25] B. Alessandro, C. Beatrice, G. Bertotti, and A. Montorsi. Domain-wall dynamics and barkhausen effect in metallic ferromagnetic materials. 2. experiments. *J. Appl. Phys.*, 68:2908–2915, 1990.
- [26] B. Alessandro, C. Beatrice, G. Bertotti, and A. Montorsi. Domain-wall dynamics and barkhausen effect in metallic ferromagnetic materials. 1. theory. *J. Appl. Phys.*, 68:2901–2907, 1990.
- [27] P. Cizeau, S. Zapperi, G. Durin, and H.E. Stanley. Dynamics of a ferromagnetic domain wall and the barkhausen effect. *Phys. Rev. Lett.*, 79:4669, 1997.
- [28] S. Zapperi, P. Cizeau, G. Durin, and E. H. Stanley. Dynamics of a ferromagnetic domain wall: Avalanches, depinning transition, and the barkhausen effect. *Phys. Rev. B*, 58:6353–6366, 1998.
- [29] Gianfranco Durin. The barkhausen effect. <http://www.iien.it/~durin/barkh.html>, 2001.
- [30] E. A. Guggenheim. The principle of corresponding states. *Journal of Chemical Physics*, 13:253–61, 1945.
- [31] P. Heller and G. B. Benedek. Nuclear magnetic resonance in MnF_2 near the critical point. *Physical Review Letters*, 8:428–32, 1962.

- [32] J. Zinn-Justin. *Quantum field theory and critical phenomena (3rd edition)*. Oxford University Press, 1996.
- [33] M. E. J. Newman. Power laws, Pareto distributions and Zipf's law. *Contemporary Physics*, 46:323–51, 2005. [arXiv.org/abs/cond-mat/0412004/](https://arxiv.org/abs/cond-mat/0412004/).
- [34] K. Dahmen and J. P. Sethna. Hysteresis, avalanches, and disorder induced critical scaling: A renormalization group approach. *Phys. Rev. B*, 53:14872, 1996.
- [35] O. Perković, K. Dahmen, and J. P. Sethna. Avalanches, barkhausen noise, and plain old criticality. *Phys. Rev. Lett.*, 75:4528, 1995.
- [36] Olga Perković, Karin A. Dahmen, and James P. Sethna. Disorder-induced critical phenomena in hysteresis: Numerical scaling in three and higher dimensions. *Phys. Rev. B*, 59:6106–19, 1999.
- [37] K. Dahmen and J. P. Sethna. Hysteresis loop critical exponents in 6-epsilon dimensions. *Phys. Rev. Lett.*, 71:3222–5, 1993.
- [38] A. Mehta, A. C. Mills, K. A. Dahmen, and J. P. Sethna. Universal pulse shape scaling function and exponents: Critical test for avalanche models applied to barkhausen noise. *Phys. Rev. E*, 65:046139/1–6, 2002.
- [39] L. Dante, G. Durin, A. Magni, and S. Zapperi. Low-field hysteresis in disordered ferromagnets. *Phys. Rev. B*, 65:144441, 2002.
- [40] D. Spasojevic, S. Bukvic, S. Milosevic, and H. E. Stanley. Barkhausen noise: Elementary signals, power laws, and scaling relations. *Phys. Rev. E*, 54:2531–2546, 1996.
- [41] M. Kuntz. *Barkhausen noise: simulations, experiments, power spectra, and two dimensional scaling*. PhD thesis, Cornell University, 1999.
- [42] G. Durin and S. Zapperi. The barkhausen effect. In G. Bertotti and I. Mayergoyz, editors, *Science of Hysteresis, Vol. II*. Elsevier, London, 2004.
- [43] M. Kuntz and J. P. Sethna. Noise in disordered systems: The power spectrum and dynamics exponents in avalanche models. *Phys. Rev. B*, 62:11699, 2000.
- [44] F. Colaiori, M. J. Alava, G. Durin, A. Magni, and S. Zapperi. Phase transitions in a disordered system in and out of equilibrium. *Phys. Rev. Lett.*, 92:257203, 2004.
- [45] Alan A. Middleton. Asymptotic uniqueness of the sliding state for charge-density waves. *Physical Review Letters*, 68:670, 1992.
- [46] A.A. Middleton and D.S. Fisher. Critical behavior of charge-density waves below threshold: numerical and scaling analysis. *Phys. Rev. B*, 47:3530–52, 1993.
- [47] O. Malcai, D. A. Lidar, O. Biham, and D. Avnir. Scaling range and cutoffs in empirical fractals. *Physical Review E*, 56:2817–28, 1997.